CHEMISTRY OF MATERIALS

pubs.acs.org/cm

Article

ScSI: A New Exfoliatable Semiconductor

Published as part of the Virtual Special Issue "John Goodenough at 100".

Austin M. Ferrenti, Maxime A. Siegler, Shiyuan Gao, Nicholas Ng, and Tyrel M. McQueen*

Cite This: https://doi.org/10.1021/acs.chemmater.2c00318

Read Online

ACCESS | Metrics & More | Article Recommendations | Supporting Information

ABSTRACT: ScSI, a missing member of the rare earth sulfoiodide (RESI) family of materials, has been synthesized for the first time. ScSI crystallizes in the FeOCl structure type, space group *Pmmn* (No. 59), a = 3.8904(2), b = 5.0732(9), c = 8.9574(6) Å. Both hyperspectral reflectance measurements and ab initio calculations support the presence of an indirect optical band gap of 2.0 eV. The bulk crystal is found to be readily exfoliatable, enabling its use as an optical component in novel heterostructures. The impact of lithium intercalation on its electronic band structure is also explored. A broader correlation is drawn between the observed structural trends in all known 1:1:1 sulfoiodide phases, cationic proportions, and electronic considerations. The realization of this phase both fills a significant synthetic gap in the literature and presents a novel exfoliatable phase for use as an optical component in next-generation heterostructure devices.

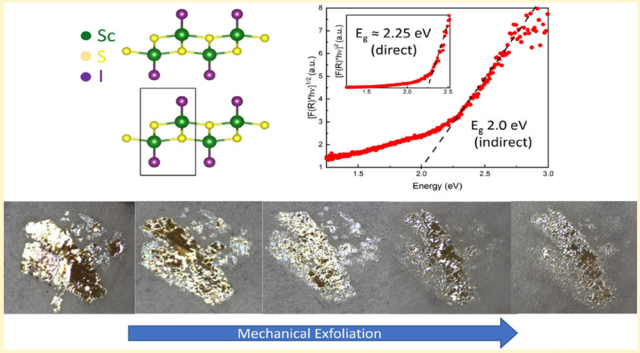

INTRODUCTION

The properties exhibited by a material system are often intricately linked to its structure, as well as how that structure evolves in response to external stimuli. Elucidation of this structure−property relationship is thus essential to understanding why a material behaves as it does. Beyond properties intrinsic to the bulk of materials themselves, layered materials have also attracted significant attention due to the van der Waals-type bonding they typically possess. These interactions are generally quite weak, allowing for simple mechanical delamination of the bulk material into uniform nanosheets, which have been observed to exhibit a large variety of phenomena distinct from their bulk analogues.[1] For phases possessing favorable optical and/or electronic properties, such as band gaps in the visible spectrum, these features can be further enhanced by the stacking of such nanosheets into larger heterostructures, which themselves can be fabricated into devices for optoelectronic applications.[2] Thus far, research in this field has focused predominantly on the development and integration of a relatively small number of materials into usable heterostructures and devices. More recently, however, more exotic phases, such as $RuCl_3$ and CrI_3,[3,4] among others,[5,6] have begun to attract more attention. Of particular interest are series of materials containing rare earth cations, as they typically possess remarkably similar physical, electronic, and magnetic properties, while also exhibiting clear structural trends. Such a trend has been observed in the RESI (RE = rare earth) family of materials, where members crystallize in three distinct structure types, based on the size of the metal cation, which may be readily interconverted with the application of pressure (Figures 1 and 2). For RE = La and Ce, containing the largest cations, the (α-CeSI) structure consists of $(RES)_n$ sheets of highly distorted, 7-coordinate metal atoms sandwiched between wrinkled iodine layers. For (β-form) CeSI and RE = Pr−Sm, the double-iodine layers instead alternate with hexagonal $(RES)_n$ sheets, containing less distorted, 7-coordinate metal atoms, owing to the smaller cation size. Finally, the smallest cations of the group, RE = Y, Gd−Lu, under standard pressure conditions crystallize in the FeOCl structure type, with $(RES)_n$ sheets of distorted octahedra again separated by double iodine layers. The FeOCl-type phases have also all been reported to exhibit paramagnetic behavior, down to 2 K, due to the presence of unpaired electrons on the rare earth cation. Upon the application of moderate pressure, the phases containing the smallest cations are observed to transition from the FeOCl structure type to the SmSI structure type, and those containing rare earth atoms of moderate size transition from the SmSI structure type to the α-CeSI structure type.[7] Further pressuring of the SmSI-type GdSI phase has been reported to induce an additional polymorphic transition, to a hexagonal $P\bar{6}$ structure.[8,9] The higher-pressure forms of

Received: January 31, 2022
Revised: May 26, 2022

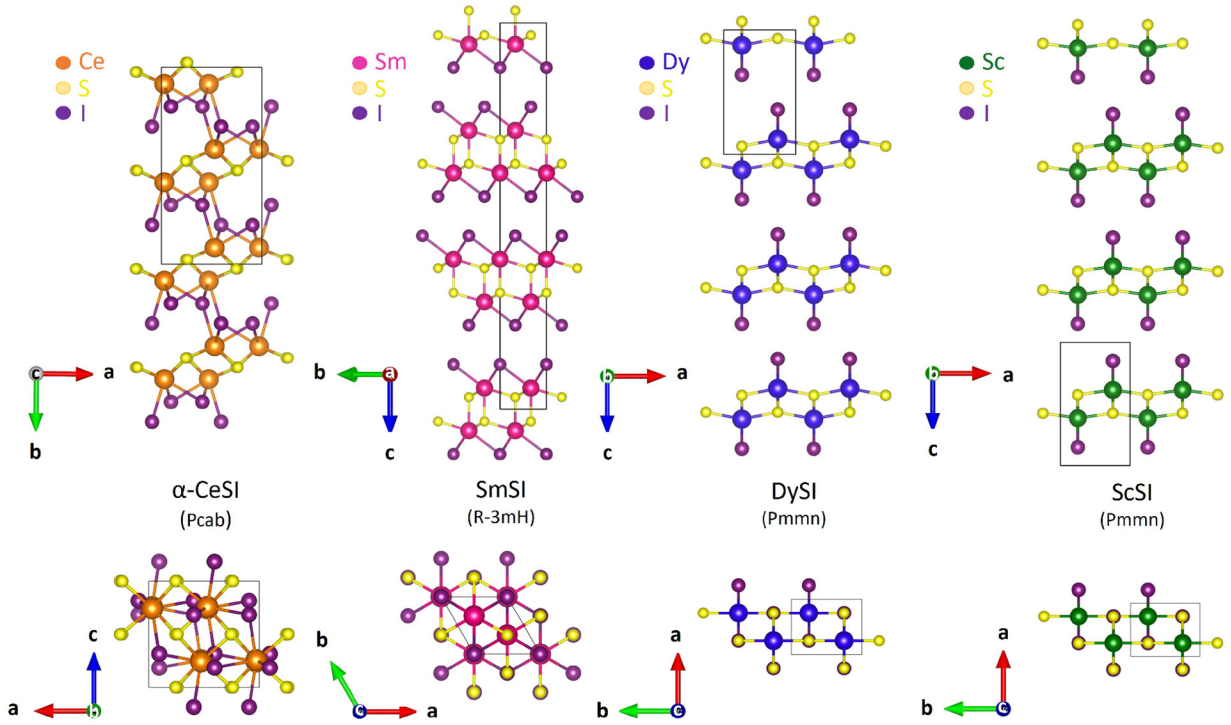

Figure 1. Comparison of the standard pressure structures of (from left to right) α-CeSI, SmSI, DySI, and ScSI (this work). The upper panels show projection of the structure along one of the nonstacking axes, while the lower panels show the projection along the stacking axis. With decreasing size of the RE cation (left to right), the structure is observed to gradually relax. Unit cells are denoted by a black box.

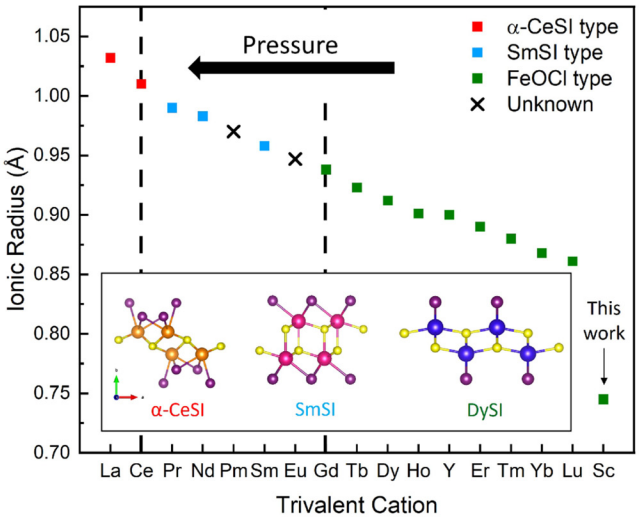

Figure 2. Structural trend across the RESI family of materials as a function of the ionic radius of the trivalent RE^{3+} cation. Phases containing the largest cations crystallize in the α-CeSI structure type, with heavily distorted metal coordination environments. Those containing cations of more moderate size crystallize in the SmSI structure type, which possesses a less distorted, but still 7-coordinate geometry. The smallest RE atoms are instead stabilized in the FeOCl structure type, with a significantly less distorted, 6-coordinate geometry. With the application of a moderate amount of pressure, the smallest members are known to undergo a phase transition to the SmSI-type structure, while the SmSI-type phases become maximally distorted in the α-CeSI geometry. ScSI is found to crystallize in the FeOCl structure type, as would be expected given its status as the smallest of the rare earth metals.

LuSI and YSI have been predicted to be strong topological insulators, with the isostructural GdSI phase being proposed as a Weyl semimetal candidate, driven by Gd magnetism.[10,11] Three members of the RESI series have yet to be reported—PmSI, EuSI, and ScSI. The realization of the Sc phase would be of particular interest, as it would represent not only the synthetic end-member of the series but also a relatively large decrease in ionic radius, relative to the current minimum, LuSI. Here we report the synthesis of this ScSI phase, briefly characterize its physical properties, and discuss its structural relationship to the existing family. Our results indicate that ScSI is a readily exfoliatable, 2.0 eV indirect band gap semiconductor warranting further study to determine its potential as an optical component in improved heterostructure devices.

METHODS

Single crystals of ScSI were initially grown by chance in the course of exploration of the Sc−Zr−S−O phase diagram; however, the synthesis is readily reproducible. In order to ensure high precursor purity, both Sc_2S_3 and ZrS_2 were synthesized from the elements. Sulfurization of Sc_2O_3 (Strem Chemical, 99.9%) proceeded by the method described by Kaneko et al.[12] Ar gas was bubbled at a rate of 1 bubble/5 s through a CS_2 (VWR, ≥99.9%) solution and flowed over Sc_2O_3 in an alumina boat for 3 h at 1100 °C. The exhaust gas was then flowed through a 1.0 M NaOH solution and neutralized. ZrS_2 was produced by a direct heating of the elements Zr (Strem Chemical, ≥99.8% foil) and S (Alfa Aesar, 99.999% pieces; repurified by low-temperature self-transport from 100 to 25 °C) in a sealed quartz tube at 200 °C/h to 900 °C for 5 days, before fast cooling at 200 °C/h to room temperature. Sc_2O_3, Sc_2S_3, and ZrS_2 were combined in a 1:1:2 molar ratio to a total composition mass of 1 g, sealed under vacuum in an 8 cm long, 16 mm OD, 14 mm ID carbon-coated quartz tube, and heated for 4 days at 1050 °C before water quenching to room temperature. The product of this initial heating was then reacted with

https://doi.org/10.1021/acs.chemmater.2c00318
Chem. Mater. XXXX, XXX, XXX−XXX

Table 1. Possible Reaction Mechanisms for the Formation of ScSI

path	reactant species	composition	transport agent	intermediate	transported product(s)
1	eqs 1−2	1:1 (mass)	I_2	Sc−Zr−I	ScSI
2	ScI_3 + Sc_2S_3	1:1 (molar)	ScI_3	Sc−I	ScI_3
3	ScI_3 + S	1:1 (molar)	ScI_3	Sc−I	ScSI (very low yield), I_2
4	Sc_2S_3 + I_2	1:1 (molar)	I_2	Sc−I	ScSI (very low yield), I_2
5	Sc_2S_3 + ZrI_4	2:1 (molar)	ZrI_4	Sc−Zr−I	ScSI (very low yield), ZrI_4, I_2

I_2 in a 1:1 mass ratio in a 15 cm long, 12 mm OD, 10 mm ID quartz tube via the chemical vapor transport (CVT) method. The source end of the tube was heated to 950 °C over 1 day, held there for 2 days, and slow cooled to room temperature over an additional two day period. The tube was positioned in the furnace such that a roughly 200 °C gradient from the source end to the cold end (950 °C → 750 °C) was produced. Large, flat, moisture-sensitive golden crystals were formed on the cold end of the tube. After transport, a white powder remained on the source end of the tube, the majority of which was identified as a rhombohedral $Zr_5Sc_2O_{13}$ phase. In order to better understand the mechanism by which ScSI is formed, several additional trials using alternative starting materials (including ScI_3 (99.999% REO basis, Alfa Aesar) and ZrI_4 (99% Alfa Aesar)) were performed under identical reaction conditions, the results of which are summarized in Table 1.

Lithium intercalation of the parent ScSI material was achieved by the lithium radical anion method using air-free techniques.[13] THF (99.7+%, Alfa Aesar) was initially dried overnight over molecular sieves (3 Å, Alfa Aesar), before the addition of benzophenone (ReagentPlus, 99%, Sigma-Aldrich) to produce a 0.2 M solution. Various quantities of Li metal were added to this reaction mixture and allowed to stir overnight until the solution became dark blue in color. Upon the addition of the ScSI parent material, the solution was allowed to stir until it became dull red in color, indicating that the majority of the radical species had been consumed. Sample A was produced by adding 0.07 g of synthesized ScSI to a 200 mL solution of 1.5:1 Li metal/benzophenone in THF and allowed to stir for 34 h with no additional heating. Sample B was produced by adding 0.50 g of synthesized ScSI to a 200 mL solution of 1.8:1 Li metal/benzophenone in THF and allowed to stir for 32 h with no additional heating.

Powder X-ray diffraction (pXRD) patterns were collected on a laboratory Bruker D8 Focus diffractometer with LynxEye detector and Cu Kα (λ = 1.5406 Å) radiation in the 2θ range from 5 to 60°. Samples were typically measured under a thin strip of transparent Scotch Magic tape, which was observed to prevent their decomposition in air on shorter time scales (<30 min). Structures were visualized with the Vesta 3 program.[14]

Prior to crystal mounting for single crystal X-ray diffraction, the crystals were quickly deposited with a small amount of Parabar 10312 oil on a microscope slide under a stream of N_2 gas to prevent crystal decomposition. A single crystal was selected, and all reflection intensities were measured at T = 110(2) K using a SuperNova diffractometer (equipped with Atlas detector) with Mo Kα radiation (λ = 0.71073 Å) under the program CrysAlisPro (Version CrysAlisPro 1.171.39.29c, Rigaku OD, 2017). The same program was used to refine the cell dimensions and for data reduction. The structure was solved with the program SHELXS-2018/3 and was refined on F^2 with SHELXL-2018/3.[15] An empirical absorption correction using spherical harmonics was applied using CrysAlisPro. The temperature of the data collection was controlled using the Cryojet system (manufactured by Oxford Instruments).

Hyperspectral reflectance measurements were conducted with a Headwall Hyperspec-VNIR/E-Series camera with a 24 mm APO Xenoplan F/2.0, VNIR lens. The samples were scanned at a speed of 1.0 mm/second under the illumination of a Headwall Model 21DC light source. Normalization was performed using light and dark references. Exfoliated specimens were produced by the scotch-tape method, with reflectance measurements performed on samples that were once-, twice-, and thrice-exfoliated, as well as on the other piece of the once-exfoliated sample.[16]

Band structure calculations were performed using the plane-wave pseudopotential method implemented in QUANTUM ESPRESSO[17] with a k-point mesh of 8 × 6 × 4. The Perdew−Burke−Ernzerhof (PBE) parametrization of the generalized gradient approximation exchange-correlation functional[18] was used, with a plane-wave cutoff of 70 Ry. The structures and cell parameters were relaxed using the DFT-D3 van der Waals functional from Grimme et al.[19] with a convergence threshold of 0.001 Ry/a.u. in force and 1 kbar in pressure. For ScSI, the relaxed lattice constants were a = 3.917 Å, b = 5.068 Å, and c = 9.031 Å. For $Li_{0.12S}ScSI$, $Li_{0.2S}ScSI$, and $Li_{0.50}ScSI$, 1/4, 1/2, and 1 Li atoms were placed into the van der Waals gap between iodine atoms in each respective unit cell, and the structure and cell parameters were relaxed while maintaining the orthorhombic structure. Li intercalation resulted in a gradual shift in the relaxed lattice constants to a = 3.925 Å, b = 5.095 Å, and c = 8.91 Å in $Li_{0.12S}ScSI$, a = 3.95 Å, b = 5.09 Å, and c = 8.94 Å in $Li_{0.25}ScSI$, and finally to a = 4.00 Å, b = 5.08 Å, and c = 8.91 Å in $Li_{0.50}ScSI$, indicating a small expansion of the lattice in the a direction. More varied shifts are observed in the c direction with increasing Li-content, but relative to the parent compound there is an overall contraction up to the maximally stuffed phase.

RESULTS AND DISCUSSION

The rather unusual method by which the title phase was produced can likely be interpreted as a consequence of the low reactivity of Sc with I_2 at elevated temperatures. Based on the observed crystalline products after heating, the route likely proceeds in two steps, shown in eq 1 and eq 2 (Path 1):

$$\text{Step 1: } 5Sc_2O_3(s) + Sc_2S_3(s) + 7ZrS_2(s) \rightarrow Zr_5Sc_2O_{13}(s) + 2ZrSO(s) + 5Sc_2S_3(s) \quad (1)$$

$$\text{Step 2: } Sc_2S_3(s) + ZrSO(s) + I_2(g) \rightarrow 2ScSI(s) + ZrS_xO_y(s) \quad (2)$$

Beyond the Sc_2S_3 precursor and $Zr_5Sc_2O_{13}$ product, the true nature of the species present after step 2 is not reliably determined from pXRD, due to the low crystallinity of the products and structural similarities among many zirconium oxysulfide/sulfate phases.

To further elucidate the mechanism by which this less direct reaction proceeds, several additional synthetic approaches were explored, all under identical reaction conditions. While the majority of reaction pathways resulted in the transport of some ScSI, crystals grown by these alternate methods were consistently smaller, thinner, and duller than those grown by the indirect method detailed above. Where ScI_3 is used as the sole transport agent, reaction with Sc_2S_3 (Path 2) yielded transport of only slightly Sc-deficient ScI_3, whereas reaction with elemental sulfur (Path 3) resulted in a low yield of transported ScSI, owing to the higher reactivity of S, relative to Sc_2S_3. In both cases, it is clear that at least at the chosen reaction temperature, ScI_3 is not a sufficiently active transport

https://doi.org/10.1021/acs.chemmater.2c00318
Chem. Mater. XXXX, XXX, XXX−XXX

agent for the production of ScSI at scale, owing to its relatively low vapor pressure. Reaction of Sc_2S_3 with I_2 (Path 4) also resulted in a low yield of dull ScSI crystals, indicating that while a Sc−I intermediate is capable of facilitating the production of ScSI, it is not sufficiently reactive, compared to Path 1.

As its presence appeared to be necessary for the measurable production of ScSI single crystals, the role of ZrS_2 in the initial reaction mixture was then investigated. The reaction of Sc_2S_3 with ZrI_4 (Path 5), which by the indirect method would be the likely Zr-based contributor to the observed transport, ultimately resulted in the transport of only a small quantity of ScSI crystals, as well as a much larger volume of ZrI_4 crystals. As ZrI_4 is significantly more volatile than ScI_3, self-transport proceeds much more quickly, leaving only the Sc−I intermediate formed at elevated temperatures to produce the small yield of ScSI crystals, as in Path 3. It is thus likely that the vapor transport process occurring by the indirect method is mediated by a gaseous Zr_xI_y phase acting as a cotransport agent. Most known zirconium sulfate and sulfide phases decompose at temperatures far below those reached in these reactions and thus would be expected to first coordinate with gaseous iodine. Relative to the other methods explored here, this enables more scandium to join a complex Sc−Zr iodide intermediate, from which the ScSI product phase can be formed, transported, and deposited. This is also supported by the presence of a zirconium iodide impurity phase in the transported products for Path 1 trials employing higher I_2 to Sc_2S_3 mass ratios. The presence of poorly crystalline, high surface area ZrS_xO_y after step 2 further helps modulate the thermodynamics by acting as a sink for the S liberated from Sc_2S_3 during the reaction.

Single-crystal diffraction measurements and subsequent refinement, the results of which are summarized in Tables 2, 3, and 4, confirmed the synthesis of a novel FeOCl-type phase with a 1:1:1 ratio of Sc:S:I. The quality of all goodness-of-fit and anisotropic displacement parameters was limited by the thin, brittle, and layered morphology, as well as moisture sensitivity, of the transported crystals. Precession images constructed from these measurements, shown in Figure 3b, exhibit minor smearing in both the (0*kl*) and (*h*0*l*) planes, whereas that of the (*hk*0) plane does not. As the latter comprises the stacking axis in the FeOCl-type, this is indicative of stacking faults in the measured representative crystal. pXRD measurements of synthesized crystals oriented along the flat face were consistent with growth along the *ab*-plane.

Table 2. ScSI Single Crystal and Structural Refinement Data

formula weight (g mol^{-1})	203.92
crystal system	orthorhombic
space group	*Pmmn* (No. 59) Origin choice #2
a (Å)	3.8904(2)
b (Å)	5.0732(3)
c (Å)	8.9574(6)
volume (Å^3)	176.97(2)
Z	2
radiation	Mo Kα (λ = 0.71073 Å)
temperature (K)	110
reflections collected/unique	3928/320
R_{int}	0.064
data/parameters	320/13
goodness-of-fit	1.162
R_1 [$F^2 > 2\sigma(F^2)$];[a] R_1 [all data]	0.0228; 0.0245
$wR(F^2)$[b]	0.0617
largest diff. peak and hole	1.12 and −1.06 e Å^{-3}

[a] $R(F) = \sum||F_o| - |F_c||/\Sigma|F_o|$. [b] $R_\omega(F_o^2) = [\sum\omega(F_o^2 - F_c^2)^2/\sum\omega(F_o^2)^2]^{1/2}$.

Table 4. ScSI Selected Bond Distances and Angles

	bond distances (Å)
Sc−S (i)	2.5833(15)
Sc−S (ii)	2.5612(3)
Sc−I	2.8660(11)
Sc−Sc (i)	3.7998(15)
Sc−Sc (ii)	3.8904(2)
	bond angles (deg)
S−Sc−S	84.78(3)
S−Sc−I	95.83(3)

ScSI crystallizes in the *Pmmn* space group, similar to the smallest members of the RESI family, as would be expected given the small size of the Sc^{3+} ion. The structure, depicted in Figure 4, consists of lightly distorted, half edge-sharing $[ScS_4I_2]^{7-}$ octahedra, which together form $(ScS)_n$ sheets with bounding iodine layers. Each scandium atom is coordinated by two iodine atoms and four sulfur atoms, the size discrepancy between which produces the deviation from true octahedral geometry. Two distinct Sc−S bonds are present in the structure, 2.5612(3) Å and 2.5833(15) Å in length, in rough agreement with that expected from the ionic radii of the Sc^{3+} (0.745 Å) and S^{2-} (1.84 Å) ions. Sc−I bond lengths agree similarly well, averaging around 2.86 Å, relative to typical values for 6-fold coordinate Sc^{3+} and I^- (2.20 Å). The layers are separated by a van der Waals gap on the order of 2.69 Å, large enough to accommodate any number of potential intercalants.

Comparison of the observed ScSI crystal structure to the known family of RESI phases, shown in Figure 1, and plotted in Figure 2 as a function of ionic radius,[20] reveals that the Sc phase is the effective low end-member of the series. The observed distortion of the metal octahedra is roughly analogous to that observed in the other FeOCl-type RESI phases; however, it is still significantly lower than in the 7-coordinate geometry of the larger-cation phases. With increasing cation radius and/or the application of pressure, iodine atoms are pushed from the minimally distorted geometry (here in ScSI), where each is coordinated by only one metal atom, to a triply coordinated state. The in-sheet Sc−S bonds are also observed to increase from 2.56 Å in ScSI to

Table 3. Atomic Positions and Anisotropic Displacement Parameters ($U_{12} = U_{23} = U_{31} = 0$)

atom	Wyckoff Site	*x*	*y*	*z*	U_{11}	U_{22}	U_{33}
Sc	2a	1/4	1/4	0.38533(16)	0.0046(5)	0.0023(5)	0.0117(6)
S	2b	1/4	−1/4	0.4249(2)	0.0046(6)	0.0018(6)	0.0107(8)
I	2b	−1/4	1/4	0.15035(5)	0.0047(2)	0.0158(3)	0.0105(3)

https://doi.org/10.1021/acs.chemmater.2c00318
Chem. Mater. XXXX, XXX, XXX−XXX

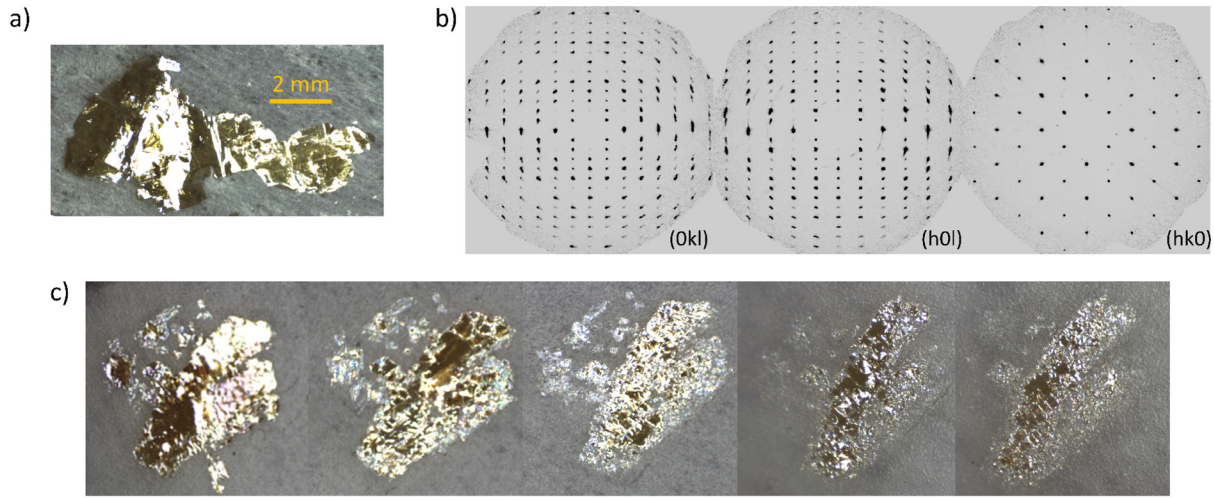

Figure 3. (a) Representative transparent, golden ScSI single crystal. (b) Calculated precession images along the (from left to right) (0*kl*), (*h*0*l*), and (*hk*0) planes. The smearing observed in both the (0*kl*) and the (*h*0*l*) planes can be attributed to stacking faults in the measured crystal. (c) Successive scotch-tape exfoliations (left to right) of a representative ScSI single crystal.

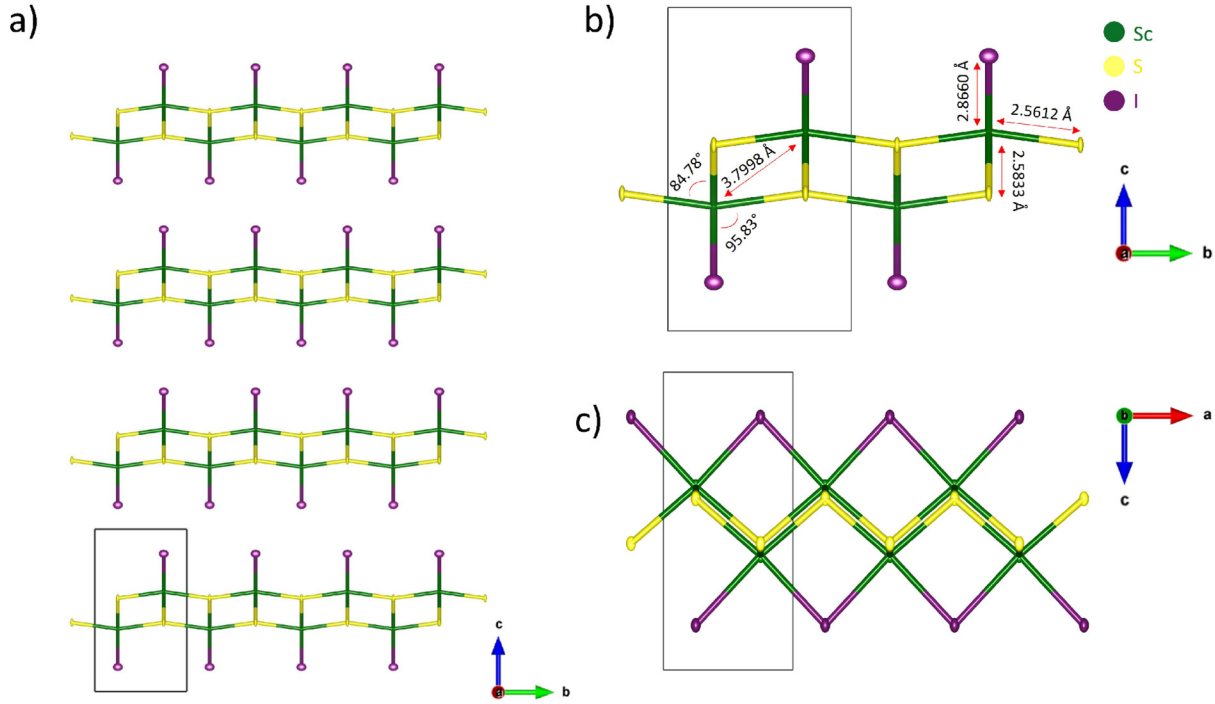

Figure 4. Crystal structure of ScSI: Sc = green, S = yellow, I = purple. Space group *Pmmn*, Origin choice #2, a = 3.8904(2), b = 5.0732(9), c = 8.9574(6) Å, V = 176.97(2) Å^3. (a) Projection showing stacking of adjacent ScSI layers along the c axis. (b) Zoomed projection along the a axis, with selected bond lengths and angles. (c) Projection along the b axis. Atoms are depicted with their anisotropic displacement ellipsoids at the 80% probability level. The unit cell is denoted by a black box.

2.86 Å in α-CeSI, as the bridging sulfur atoms experience increasing repulsion from the interlayer iodine atoms. As neighboring $(RES)_n$ sheets are pushed closer together, the van der Waals gap is bridged, and the structure becomes entirely three-dimensional.

Two other 1:1:1 sulfoiodide phases, SbSI and BiSI, are known to exist and have been intensely studied over the years due to their ferroelectric and semiconducting natures.[21,22] In the paraelectric phase, both crystallize in the *Pnma* space group and consist of strongly bonded $[Sb_2S_2I_2]_n/[Bi_2S_2I_2]_n$ chains, with weak interchain van der Waals interactions.[23,24] While not directly analogous to the RESI series, the expected ionic radii of Sb^{3+} and Bi^{3+} cations would suggest a 6- and 7-fold coordination, in line with the FeOCl and α-CeSI structure types, respectively. However, both are found to be 5-fold coordinate. Deviations from Vegard's law in solid solutions of the two materials have been attributed to the presence of the lone pairs present on the metal cations, which may also prevent their adherence to the structural trends observed in the RESI materials.[25]

Whereas the structure of the pnictide sulfoiodide phases is likely additionally distorted by the considerable steric effects about the metal cation, the observed volatility and low synthetic yield by direct methods of the scandium member

https://doi.org/10.1021/acs.chemmater.2c00318
Chem. Mater. XXXX, XXX, XXX−XXX

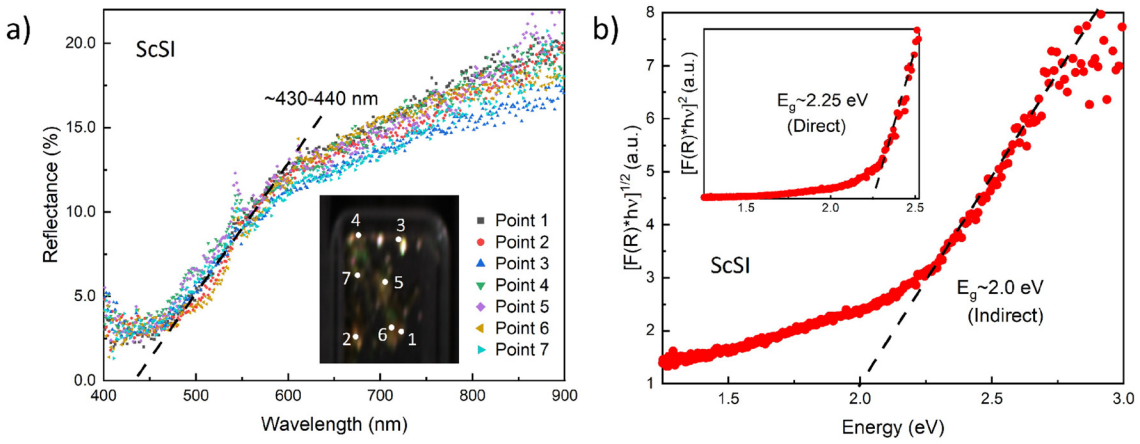

Figure 5. (a) Hyperspectral reflectance spectra of representative ScSI single crystals. Each data set corresponds to the reflectance of a randomly sampled crystal in the distribution. (b) Kubelka–Munk-transformed reflectance spectra from which the indirect (main) and direct (inset) optical bandgaps were derived.

suggest that this phase may demonstrate the opposite effect. From La^{3+} to Lu^{3+} (Y^{3+} inclusive), there is a relatively gradual, stepwise decrease in cationic radius, while the difference between Lu^{3+} and Sc^{3+} is significantly larger. The distortion of the Sc octahedra in FeOCl-type ScSI is insufficiently large to induce a transition to a higher-coordinate environment, but Sc^{3+} is still large enough to produce a stable phase with the significantly larger S^{2-} and I^-, whereas no smaller trivalent cation-containing phases with this composition are known to exist. ScSI thus likely represents not only a synthetic minimum in the RESI family but also in the broader sulfoiodide phase space. A more complete view of the structural trends across this family of materials would be enabled by future studies into whether the ScSI system undergoes structural phase transitions at higher pressures, as its siblings do. If this structural transition is accompanied by a topological phase transition, as with the Gd, Y, and Lu analogues, characterization and study of its surface states would also be of interest.

Due to the layered morphology of the transported crystals, they were also found to be easily exfoliatable via the scotch-tape method, as shown in Figure 3c. While the exfoliation of other RESI members has not yet been reported, a recent study demonstrated that bulk crystals of the closely related SbSI phase could be easily delaminated via the liquid exfoliation method.[26] In addition, both the isostructural HoSI and DySI were identified in the NIST JARVIS-DFT repository as possessing relatively low calculated exfoliation energies of 55.48 meV/atom and 55.68 meV/atom, respectively.[27] The Ho-, Dy-, and SmSI phases were also included in a broad review of predicted two-dimensional materials by Mounet et al.[28] As the exfoliation energy of graphene layers from a bulk graphite surface has been estimated to be 55.16 meV/atom,[29] this suggests that at least the FeOCl-type members of the RESI family may be viably exfoliatable 2.0 eV indirect band gap candidates for integration into novel heterostructures.

In order to probe the optical band gap of ScSI, hyperspectral reflectance measurements were performed on a representative distribution of synthesized single crystals. Point spectra for seven distinct specimens are shown in Figure 5a and are observed to be in good agreement with one another. A Kubelka–Munk transform was then applied to the spectrum collected at one such point and the slope of the resulting curve used to derive the optical band gap of the material (Figure 5b).[30,31] Plotting the square root product of the energy and the Kubelka–Munk function ($\gamma = 1/2$) reveals an indirect optical transition on the order of 2.00 eV, while a direct gap of about 2.25 eV is derived from the square product of the two ($\gamma = 2$) (inset), the former being consistent with its gold color. Point spectra of several exfoliated samples were also collected, and Kubelka–Munk transforms of the collected data are shown in Figure S2. With decreasing sample thickness, there is a general increase in both the derived direct and indirect band gap widths; however, these results were observed to be somewhat variable. Due to the large optical absorbance exhibited by this material below its band gap, the brittle morphology and moisture sensitivity of the transported crystals, and the subsequent difficulty associated with obtaining an accurate measure of its exfoliated thickness, we conclude only a broader trend toward a larger band gap with further exfoliation, similar to that observed in MoS_2.[32]

Due to the observed tendency of some FeOCl-type materials to become superconducting upon the introduction of electron donor species into the interlayer gap,[33,34] lithium intercalation of the synthesized ScSI phase was attempted via the lithium-benzophenone radical anion method. Several positive signs of lithium having been partly incorporated into the structure were observed, such as a gradual change in color from golden to metallic bluish on the surface for both compositions, as well as a broadening of and slight shift in the positions of pXRD reflections (Figure S1); however, no superconductivity was observed. While pXRD is not a reliable technique for quantitive analysis of lithium content in intercalated phases, due to the small size of the Li^+ ion, we attempted to obtain an approximate estimate for our higher-doped composition by comparison to the existing literature. In the case of lithium-intercalated β-ZrNCl, Yamanaka et al. observed a clear leftward shift in all [00l] reflections, relative to the parent compound, corresponding to an increase in the interplanar spacing.[35] For their reported $Li_{0.16}ZrNCl$ phase, the third (009) and fourth (0012) most intense reflections are shifted by approximately 0.32 and 0.50 Å, respectively, toward higher d-spacing. In our Sample B, we observe approximately 0.07 and 0.12 Å shifts in the (003) and (004) reflections, relative to ScSI, to higher d-spacing. While not directly analogous in terms of the parent structures or the bounding halogen at each interstitial site, an approximate comparison of the shifts observed in the two

https://doi.org/10.1021/acs.chemmater.2c00318
Chem. Mater. XXXX, XXX, XXX−XXX

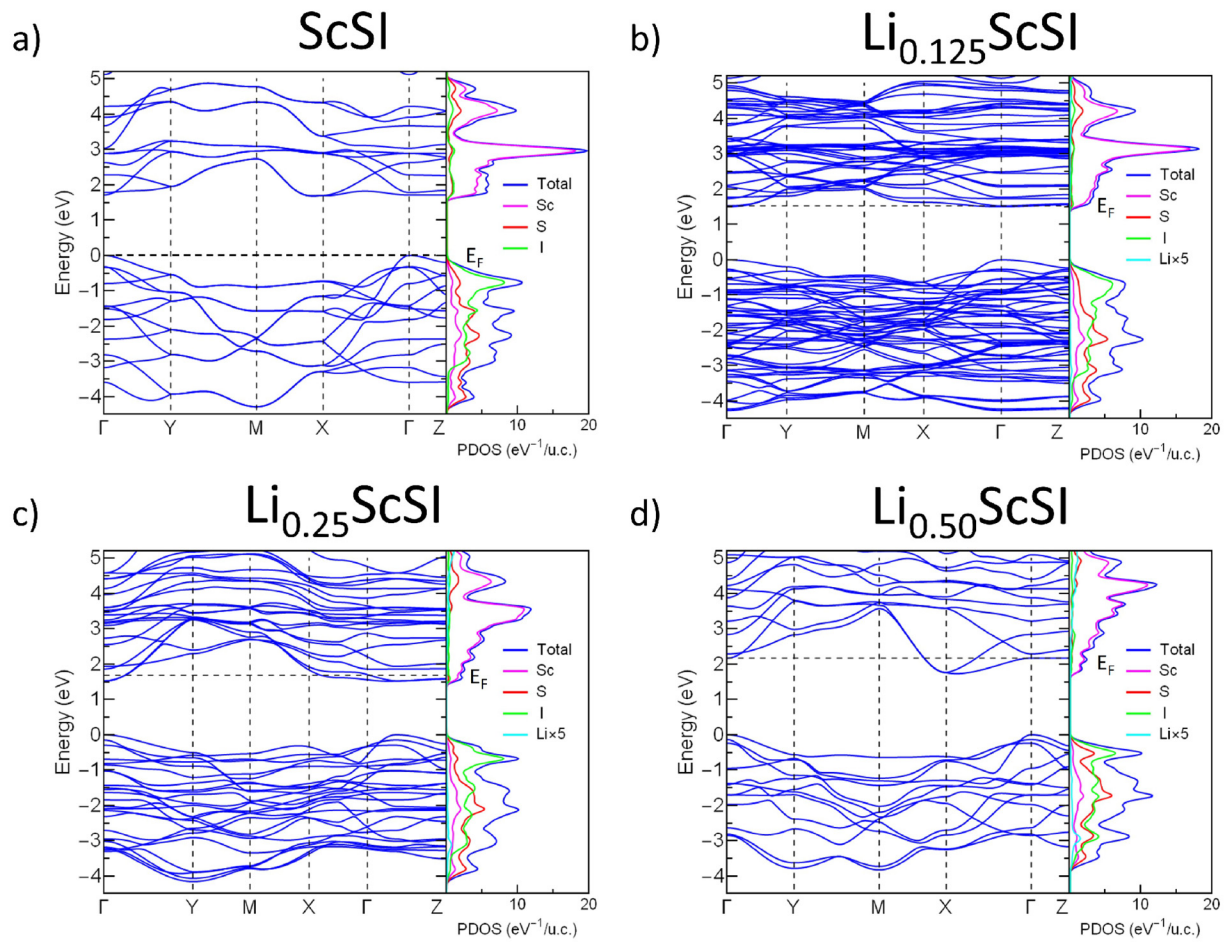

Figure 6. Representative band structure calculations of (a) stoichiometric ScSI and theoretical Li-intercalated analogues, containing (b) 1/8, (c) 1/4, and (d) 1/2 molar equivalents of lithium per formula unit. This corresponds to compositions containing 0, 1/4, 1/2, and 1 Li atoms per unit cell, respectively. The addition of Li to a structure typically follows the rigid band model. The Li density of states in parts (b)−(d) has been scaled by a factor of 5 for clarity.

materials suggests a Li filling in our material about 23% of that in the β-ZrNCl intercalate. This would represent a filling of 0.03−0.04 mol equiv per formula unit in our more-intercalated Sample B. In our Sample A, there is no visible shift in the (003) or (004) reflections, relative to those observed in the parent ScSI, suggesting that the filling is likely even lower, where the relatively minimal lithium uptake into the van der Waals gap is not sufficient to produce any significant expansion of the interlayer spacing. Future studies should focus on where chemical and pressure tuning can induce superconductivity in a lithium-intercalated analogue of ScSI.

Ab initio band structure calculations of unlithiated ScSI (Figure 6a) predict a direct band gap on the order of 1.7 eV at the Γ point, which is slightly lower than that derived from the reflectance measurements but is reasonable based on the gold color of the transported crystals and the tendency of DFT calculation methods to underestimate experimental band gaps. Due to the high degree of difficulty associated with reducing trivalent scandium, the maximum amount of lithium that may be feasibly intercalated into the parent phase is likely quite small (<1/8 mol equiv), with the intercalated analogues maintaining the FeOCl-structure type. However, to better understand the impact of electron-doping on the electronic structure of this material, subsequent calculations of several theoretical lithium-intercalated ScSI phases (Figures 6b−d), containing 1/4, 1/2, and 1 Li atoms per unit cell, respectively, were also performed. For the lowest of these fillings, corresponding to a $Li_{0.125}ScSI$ phase (Figure 6b), there is only a shift in the Fermi energy to the conduction band minimum, as expected by the electron-donating nature of the intercalant to the Sc d-orbitals. Our estimate of lithium content for the higher-doped Sample B (0.03−0.04 mol equiv per formula unit), which would result in even less electron density added to the conduction band than in the theoretical $Li_{0.125}ScSI$ phase, is thus reasonable, given the similarity of its paramagnetic response to that of ScSI. Sample A, containing less lithium per formula unit still, would also not be expected to exhibit radically different magnetic behavior than the parent material. For both samples, the gradual color change observed to a metallic blue can be understood as a result of increasing donation of electrons to the Sc d-orbitals and subsequent increasing metallicity of the compositions, albeit to a lesser extent than is observed in the calculated band structure for $Li_{0.125}ScSI$. For the two higher-filled theoretical phases, $Li_{0.25}ScSI$ (Figure 6c) and $Li_{0.50}ScSI$ (Figure 6d), Fermi energies 0.20 and 0.40 eV above the conduction band minimum are predicted, in line with increasing metallicity of the intercalated structures. For the latter, bands at the Fermi level are also observed to be exceptionally flat from Γ to Z, a feature which is common among many layered phases.[34] A

https://doi.org/10.1021/acs.chemmater.2c00318
Chem. Mater. XXXX, XXX, XXX−XXX

slight broadening of the conduction bands is observed, which we attribute to the small expansion of the *a*-axis and contraction of the *b*-axis, evident in the relaxed lattice parameters, with increasing lithium content. Finally, the overall band shapes also remain largely unchanged, relative to the host material, in line with the rigid band model.[36]

CONCLUSION

In conclusion, we present a novel method for the synthesis of ScSI, an unreported member and effective lower compositional limit of the RESI family of materials. From this smallest member, where the Sc octahedra are the least heavily distorted, increasing size of the metal cation is accompanied by further coordination and distortion of its coordination environment, as well as structural transitions from the orthorhombic FeOCl-type (space group *Pmmn*), to the hexagonal SmSI-type (space group $R\bar{3}m$), and finally to the orthorhombic α-CeSI-type (space group *Pcab*). In tuning pressure, the ease with which many of these phases may transition between the structure types highlights the importance of steric effects across the chemically similar family of rare earth sulfoiodides. Synthesis of the Eu analogue would allow for a more complete understanding of the structural trend across the series, as well as provide additional insight into whether past difficulties in its synthesis could be attributed to thermodynamic instabilities, as was likely the case for ScSI or to low precursor reactivity. We also determine the optical band gap of ScSI via both direct and ab initio methods and observe good agreement between the two. Based on our successful mechanical exfoliation trials, liquid-phase exfoliation of ScSI, or its lithium intercalate, is likely to result in the production of uniform nanosheets. Our results thus suggest ScSI as an easily exfoliatable, visible light band gap material, the application of which in novel heterostructures has the potential to improve optoelectronic devices.

ASSOCIATED CONTENT

Supporting Information

The Supporting Information is available free of charge at https://pubs.acs.org/doi/10.1021/acs.chemmater.2c00318.

pXRD patterns of bulk and lithium-intercalated ScSI crystals and hyperspectral reflectance data obtained from several exfoliated ScSI crystals (PDF)

AUTHOR INFORMATION

Corresponding Author

Tyrel M. McQueen − *Department of Chemistry, Institute for Quantum Matter, William H. Miller III Department of Physics and Astronomy, and Department of Materials Science and Engineering, The Johns Hopkins University,, Baltimore, Maryland 21218, United States;* orcid.org/0000-0002-8493-4630; Email: mcqueen@jhu.edu

Authors

Austin M. Ferrenti − *Department of Chemistry and Institute for Quantum Matter, William H. Miller III Department of Physics and Astronomy, The Johns Hopkins University,, Baltimore, Maryland 21218, United States*

Maxime A. Siegler − *Department of Chemistry, The Johns Hopkins University,, Baltimore, Maryland 21218, United States;* orcid.org/0000-0003-4165-7810

Shiyuan Gao − *Institute for Quantum Matter, William H. Miller III Department of Physics and Astronomy, The Johns Hopkins University,, Baltimore, Maryland 21218, United States;* orcid.org/0000-0002-9069-5306

Nicholas Ng − *Department of Chemistry and Institute for Quantum Matter, William H. Miller III Department of Physics and Astronomy, The Johns Hopkins University,, Baltimore, Maryland 21218, United States*

Complete contact information is available at: https://pubs.acs.org/10.1021/acs.chemmater.2c00318

Notes

The authors declare no competing financial interest.

The data underlying this study are openly available at the online repository https://doi.org/10.34863/3jft-j385.

ACKNOWLEDGMENTS

This work was funded by the National Science Foundation Division of Materials Research under Award No. DMR-1905411. The hyperspectral data was collected as part of a commissioning experiment within the National Science Foundation Materials Innovation Platform PARADIM, under Cooperation Agreement No. 2039380. Calculations were performed using computational resources of the Maryland Advanced Research Computing Center and the Advanced Research Computing at Hopkins (ARCH) Rockfish cluster. The Rockfish cluster is supported by the National Science Foundation Award No. OAC-1920103.

REFERENCES

(1) Zhan, H.; Guo, D.; Xie, G. Two-dimensional layered materials: from mechanical and coupling properties towards applications in electronics. *Nanoscale* **2019**, *11*, 13181−13212.

(2) Li, M.-Y.; Chen, C.-H.; Shi, Y.; Li, L.-J. Heterostructures based on two-dimensional layered materials and their potential applications. *Mater. Today* **2016**, *19*, 322−335.

(3) Weber, D.; Schoop, L.-M.; Duppel, V.; Lippmann, J. M.; Nuss, J.; Lotsch, B. V. Magnetic properties of restacked 2D spin 1/2 honeycomb $RuCl_3$ nanosheets. *Nano Lett.* **2016**, *16*, 3578−3584.

(4) Huang, B.; Clark, G.; Navarro-Moratalla, e.; Klein, D. R.; Cheng, R.; Zhong, D.; Schmidgall, E.; McGuire, M. A.; Cobden, D. H.; Seyler, K. L.; et al. Layer-dependent ferromagnetism in a van der Waals crystal down to the monolayer limit. *Nature* **2017**, *546*, 270−273.

(5) Li, H.; Lu, G.; Wang, Y.; Yin, Z.; Cong, C.; He, Q.; Wang, L.; Ding, F.; Yu, T.; Zhang, H. Mechanical exfoliation and characterization of single-and few-layer nanosheets of WSe_2, TaS_2, and $TaSe_2$. *Small* **2013**, *9*, 1974−1981.

(6) Jha, R. K.; Guha, P. K. Liquid exfoliated pristine WS_2 nanosheets for ultrasensitive and highly stable chemiresistive humidity sensors. *Nanotechnology* **2016**, *27*, 475503.

(7) Dagron, C.; Etienne, J.; Flahaut, J.; Julien-Pouzol, M.; Laruelle, P.; Rysanek, N.; Savigny, N.; Sfez, G.; Thevet, F. Fluorosulfides, Sulfobromides, and Sulfoiodides of the Rare Earth Elements. *Proceedings of the 8th Rare Earth Research Conference*; Bureau of Mines, US Department of the Interior: 1970; pp 127−139.

(8) Beck, H. P.; Strobel, C. Zur Hochdruckpolymorphie der Seltenerdsulfidiodide LnSI. *Z. Anorg. Allg. Chem.* **1986**, *535*, 229−239.

(9) Blaschkowski, B.; Rosner, H.; Schnelle, W.; Schleid, T. Sulfidiodide (MSI) der schweren Lanthanoide (M = Gd - Lu): Kristallstrukturen und magnetische Eigenschaften. *Z. Anorg. Allg. Chem.* **2013**, *639*, 237−240.

(10) Nie, S.; Xu, G.; Prinz, F. B.; Zhang, S.-C. Topological semimetal in honeycomb lattice LnSI. *Proc. Natl. Acad. Sci. U.S.A.* **2017**, *114*, 10596−10600.

(11) Zou, J.; He, Z.; Xu, G. The study of magnetic topological semimetals by first principles calculations. *NPJ. Comput. Mater.* **2019**, *5*, 96.
(12) Kaneko, T.; Yashima, Y.; Ahmadi, E.; Natsui, S.; Suzuki, R. O. Synthesis of Sc sulfides by CS_2sulfurization. *J. Solid State Chem.* **2020**, *285*, 121268.
(13) Golden, J. H.; DiSalvo, F. J.; Frechet, J. M. Room-temperature synthesis of $(LiM_{o_3}Se_3)_n$ and the determination of the relative reduction potential of tert-butyllithium. *Chem. Mater.* **1994**, *6*, 844−849.
(14) Momma, K.; Izumi, F. VESTA 3 for three-dimensional visualization of crystal, volumetric and morphology data. *J. Appl. Crystallogr.* **2011**, *44*, 1272−1276.
(15) Sheldrick, G. M. Crystal structure refinement with SHELXL. *Acta Crystallogr. C Struct. Chem.* **2015**, *71*, 3−8.
(16) Yi, M.; Shen, Z. A review on mechanical exfoliation for the scalable production of graphene. *J. Mater. Chem. A* **2015**, *3*, 11700−11715.
(17) Giannozzi, P.; Baroni, S.; Bonini, N.; Calandra, M.; Car, R.; Cavazzoni, C.; Ceresoli, D.; Chiarotti, G. L.; Cococcioni, M.; Dabo, I.; et al. QUANTUM ESPRESSO: a modular and open-source software project for quantum simulations of materials. *J. Phys.: Condens. Matter* **2009**, *21*, 395502.
(18) Perdew, J. P.; Burke, K.; Ernzerhof, M. Generalized gradient approximation made simple. *Phys. Rev. Lett.* **1996**, *77*, 3865.
(19) Grimme, S.; Antony, J.; Ehrlich, S.; Krieg, H. A consistent and accurate ab initio parametrization of density functional dispersion correction (DFT-D) for the 94 elements H-Pu. *J. Chem. Phys.* **2010**, *132*, 154104.
(20) Shannon, R. D. Revised effective ionic radii and systematic studies of interatomic distances in halides and chalcogenides. *Acta Crystallogr.* **1976**, *32*, 751−767.
(21) Nitsche, R.; Roetschi, H.; Wild, P. New ferroelectric V. VI. VII compounds of the SbSI type. *Appl. Phys. Lett.* **1964**, *4*, 210−211.
(22) Xu, Z.; Fong, C.; Wooten, F.; Yeh, Y. Reflectance ellipsometry studies of the ternary chalcohalides SbSI, SbSeI and BiSI near room temperature. *Ferroelectrics* **1984**, *56*, 187−202.
(23) Haase-Wessel, W. Die Kristallstruktur des Wismutsulfidjodids (BiSJ). *Sci. Nat.* **1973**, *60*, 474−474.
(24) Kikuchi, A.; Oka, Y.; Sawaguchi, E. Crystal structure determination of SbSI. *J. Phys. Soc. Jpn.* **1967**, *23*, 337−354.
(25) Groom, R. A.; Jacobs, A.; Cepeda, M.; Drummey, R.; Latturner, S. E. Structural and optical properties of Sb-substituted BiSI grown from sulfur/iodine flux. *Inorg. Chem.* **2017**, *56*, 12362−12368.
(26) Wang, C.; Xiao, X.; Zhu, H.; Wang, Y.; Du, X.; Yang, Z.; Duan, R.; et al. Nonlinear Optical Response of SbSI Nanorods Dominated with Direct Band Gaps. *J. Phys. Chem. C* **2021**, *125*, 15441−15447.
(27) Choudhary, K.; Kalish, I.; Beams, R.; Tavazza, F. High-throughput identification and characterization of two-dimensional materials using density functional theory. *Sci. Rep.* **2017**, *7*, 5179.
(28) Mounet, N.; Gibertini, M.; Schwaller, P.; Campi, D.; Merkys, A.; Marrazzo, A.; Sohier, T.; Castelli, I. E.; Cepellotti, A.; Pizzi, G.; et al. Two-dimensional materials from high-throughput computational exfoliation of experimentally known compounds. *Nat. Nanotechnol.* **2018**, *13*, 246−252.
(29) Chen, X.; Tian, F.; Persson, C.; Duan, W.; Chen, N. Interlayer interactions in graphites. *Sci. Rep.* **2013**, *3*, 3046.
(30) Tran, T. T.; Panella, J. R.; Chamorro, J. R.; Morey, J. R.; McQueen, T. M. Designing indirect-direct bandgap transitions in double perovskites. *Mater. Horizons* **2017**, *4*, 688−693.
(31) Makula, P.; Pacia, M.; Macyk, W. How to correctly determine the band gap energy of modified semiconductor photocatalysts based on UV-Vis spectra. *J. Phys. Chem. Lett.* **2018**, *9*, 6814−6817.
(32) Neville, R.; Evans, B. The Band Edge Excitons in 2H-MoS_2. *Phys. Status Solidi (B): Basic Res.* **1976**, *73*, 597−606.
(33) Fogg, A.; Green, V.; et al. Superconducting intercalation compounds of metal nitride halides. *J. Mater. Chem.* **1999**, *9*, 1547−1551.
(34) Yamanaka, S.; Yasunaga, T.; Yamaguchi, K.; Tagawa, M. Structure and superconductivity of the intercalation compounds of TiNCl with pyridine and alkali metals as intercalants. *J. Mater. Chem.* **2009**, *19*, 2573−2582.
(35) Yamanaka, S.; Kawaji, H.; Hotehama, K.-i; Ohashi, M. A new layer-structured nitride superconductor. Lithium-intercalated β-zirconium nitride chloride, Li_xZrNCl. *Adv. Mater.* **1996**, *8*, 771−774.
(36) Cohen, M.; Heine, V. Electronic band structures of the alkali metals and of the noble metals and their α-phase alloys. *Adv. Phys.* **1958**, *7*, 395−434.

https://doi.org/10.1021/acs.chemmater.2c00318
Chem. Mater. XXXX, XXX, XXX−XXX

Supporting Information for

ScSI: A new exfoliatable semiconductor

Austin M. Ferrenti,[†,‡] Maxime A. Siegler,[†] Shiyuan Gao,[‡] Nicholas Ng,[†,‡] and Tyrel M. McQueen[*,†,‡,¶]

†*Department of Chemistry, The Johns Hopkins University, Baltimore, MD 21218, USA*

‡*Institute for Quantum Matter, William H. Miller III Department of Physics and Astronomy, The Johns Hopkins University, Baltimore, Maryland 21218, USA*

¶*Department of Materials Science and Engineering, The Johns Hopkins University, Baltimore, MD 21218, USA*

E-mail: mcqueen@jhu.edu

pXRD patterns of bulk and lithium-intercalated ScSI

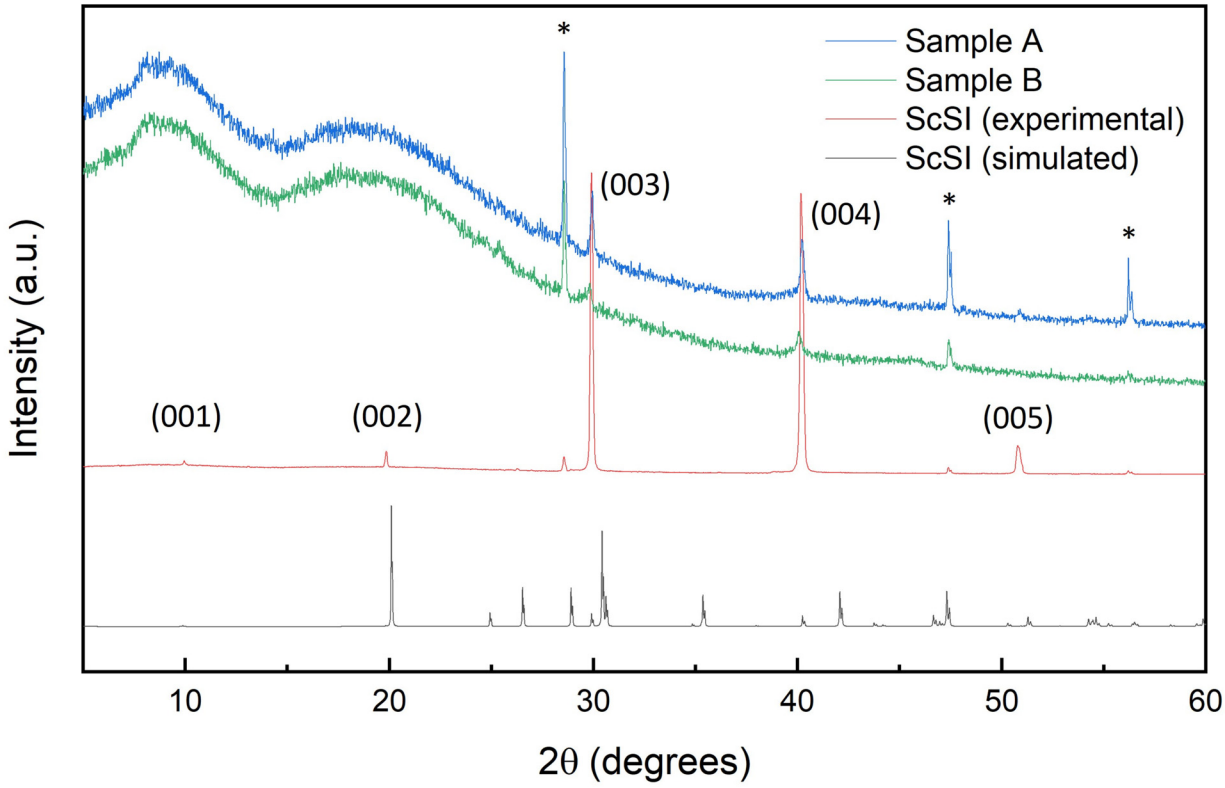

Figure S1: pXRD patterns of simulated (black) and synthesized bulk ScSI (red), as well as intercalated Sample A (blue) and Sample B (green) from $2\theta = 5$ to 60 degrees. The measurements were performed with the synthesized crystals laid flat and taped to the sample holder with a small quantity of silicon for standardization of reflection positions (denoted by *). Strong preferred orientation is observed for all (00l) reflections. A slight leftward shift in reflection positions is observed for only Sample B, indicative of an expansion of the unit cell along the c-axis.

Exfoliated ScSI hyperspectral data

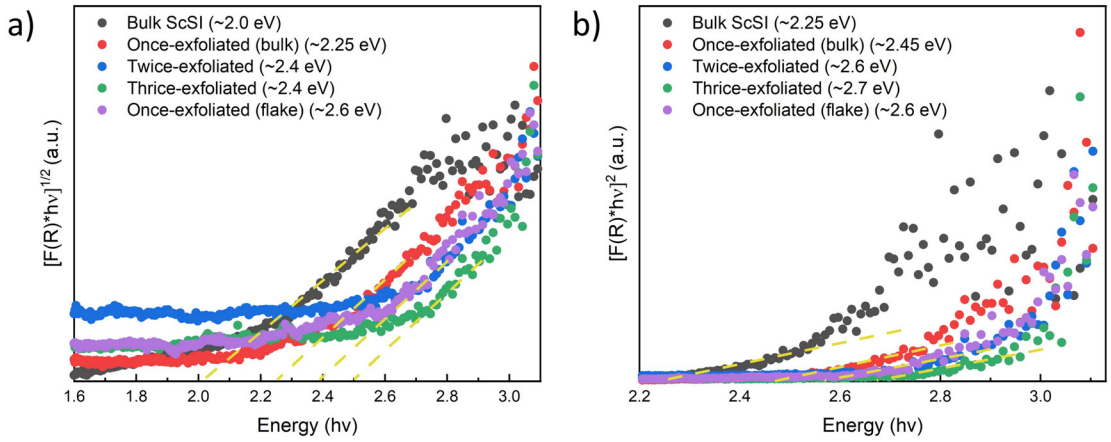

Figure S2: a) Kubelka-Munk-transformed reflectance spectra from which the a) indirect and b) direct optical bandgaps were derived for representative bulk (black), once-exfoliated (bulk-red, flake-purple), twice-exfoliated (blue), and thrice-exfoliated (green) ScSI crystals.